Eur. Phys. J. D (2016) 70: 92
DOI: 10.1140/epjd/e2016-70061-5

THE EUROPEAN PHYSICAL JOURNAL D

Regular Article

On spatial stabilization of dielectric barrier discharge microfilaments by residual heat build-up in air*

Jozef Ráhel[1,a], Zsolt Szalay[2], Jan Čech[1], and Tomáš Morávek[1]

[1] Masaryk University, Department of Physical Electronics, 611 37 Brno, Czech Republic
[2] Comenius University, Department of Experimental Physics, 842 48 Bratislava, Slovakia

Received 30 January 2016 / Received in final form 11 March 2016
Published online 19 April 2016 – © EDP Sciences, Società Italiana di Fisica, Springer-Verlag 2016

Abstract. Microfilaments of dielectric barrier discharge are known for their multiple re-appearance at the same spot on dielectrics. This effect of localized re-appearance is driven by residual excited species and ions, surface charge deposited on the dielectric and the local temperature build-up resulting in the local increase of reduced electric field $E/\Delta N$. To assess the magnitude of the latter, the breakdown voltage vs. temperature up to 180 °C was carefully measured at coplanar DBD and used as an input into the numerical simulation of heat build-up by the train of discharge pulses. An average reduction of breakdown voltage was found to be 20 V/K. The model predicted a quasi-stable microfilament temperature into which the thermal build-up rapidly converges. Its magnitude agreed well with the reported rotational temperature of similar electrode configuration. The impact of quasi-stable temperature on microfilament formation dynamics is further discussed.

1 Introduction

Spatial stabilization, i.e. localized re-appearance, of dielectric barrier discharge (DBD) microfilaments represents an inherent and technologically unwelcomed phenomenon responsible for non-uniform plasma treatment leading eventually to material pinholing. In connection to the problem of material pinholing it is important to realize that the energy released by a single occurrence of DBD microdischarge is quite small (in air: 0.1 nC $\sim 10^{-6}$ J). Taking into account the heat capacity of typical polymer materials, microdischarge must repeatedly strike the same spot on material for considerable number of times (10^2–10^3), in order to cause some detectable thermal damage. Therefore any reduction in the number of localized re-appearance would have positive effect on the output of DBD treatment of heat sensitive materials or on better macroscopic uniformity of treated surface.

The physics behind the localized re-occurrence of volume DBD microfilament in air was thoroughly analyzed in works of Akishev et al. [1–3]. They concluded that the spatial "memory" of microdischarges originates from a local reduction of inception voltage caused by the combination of two effects: slow recombination of plasma species created within the microdischarge channel (microfilament) and the surface charge left by microdischarge on the dielectric barrier. The former effect is consistent with our common laboratory experience that the increase of driving frequency (i.e. shortening the time lag between two consequent micro-breakdowns) makes the spatial stabilization more pronounced. Latter effect is claimed to be responsible only for the time jitter of micro-breakdown and its magnitude. This was a novel insight into the process, which slightly contradicted the so far generally accepted opinion that the surface memory charge played a primary role in microdischarge spatial stabilization [4,5].

Spatial stabilization of DBD microfilaments occurs also in DBD with coplanar geometry electrodes. One of the authors' (Čech) recent time-correlated visual and electrical measurements of coplanar DBD microfilaments revealed that the number of detected current pulses exceeded the number of observed microfilaments [6]. The difference rose for wider inter-electrode gaps. A natural explanation is the presence of multiple breakdowns within the same microdischarge channel. Multiple breakdowns, however, cannot be caused by surface charge, since it is reducing the instantaneous local electric field. It must be related to effect of volume residuals from decayed plasma channel, namely to either of: (1) enhanced number of seed electrons arising e.g. from negative ion electron detachment, Penning ionization etc.; (2) increase

* Contribution to the Topical Issue "Recent Breakthroughs in Microplasma Science and Technology", edited by Kurt Becker, Jose Lopez, David Staack, Klaus-Dieter Weltmann and Wei Dong Zhu.

[a] e-mail: rahel@mail.muni.cz

of first ionization coefficient α due to local rise of temperature, which provides local growth of reduced electric field $E/\Delta N$ [7]. Owing to the slow rate of radial diffusion losses with respect to the typical DBD frequencies, both contributions of (1) and (2) display a substantial cumulative effect. Hence the multiple breakdowns are an inevitable consequence of localized re-appearance and provide further positive feedback to its spatial stabilization. At the same time, the very existence of multiple breakdowns provide a valuable information on the relative importance of acting forces – local enhancement of gas ionization due to cumulative effects is greater than the electric field reduction from deposited surface charge.

Our work presented in this article is focused on evaluating the actual effect of local temperature increase on microfilament stabilization. An interesting feature of the temperature increase has practically no dependence on chemical kinetics involved within the microfilament. Therefore it can provide information on the fundamental minimum of stationary appearance of filamentary DBD regime. Thermally induced reduction of E/N was studied mainly in the connection with repetitive nanosecond pulsed sparks [8,9], or sparks in general [10]. While similar in their timescale and repetition rate, pulsed sparks are distinct from DBD microdischarges by their considerably higher amount of energy being released. Akishev et al. [3] implemented ohmic heating and diffusive losses to their numerical model of DBD microdischarge to account for some temperature changes. But their impact on local reduction of E/N was not discussed there. With respect to the DBD formation dynamics it is important to realize, that even 1% of local breakdown voltage reduction (i.e. ∼100 V in air) makes a significant time advantage over adjacent locations. At the time of electrode polarity reversal, where the breakdown of continuously powered DBD typically occurs, this represents up to 100 ns head start on adjacent microdischarge. Formation of those would be consequently hampered by already deposited surface charge of the favoured microdischarge, whose lifetime in air is only in the order of tens of nanoseconds. Therefore, the knowledge of actual reduction of E/N by a single DBD microdischarge is an important prerequisite for any further analysis.

Simulations of microdischarge formation in different DBD geometries presented in reference [11] had shown that maximum energy is released near the vicinity of electrodes – at cathode layer for volume DBD, or at both cathode and anode layer for coplanar DBD. Since the thermal conductivity of common DBD dielectrics is $\sim 10^3$ greater than the conductivity of gases, a close proximity of dielectrics to the microdischarge channel (microfilament) may provide more rapid heat dissipation and suppress the effect of localized re-appearance. This is true especially for coplanar DBD (or surface DBD in general) where microfilaments are formed along the dielectric surface. Therefore, the knowledge of actual role of dielectric boundary played in local temperature build-up is important as well.

Our paper presents a simple yet straightforward approach to assess the contribution of local rise of temperature of localized re-appearance in air coplanar DBD. High speed camera was used to measure average residence time of spatially stabilized microdischarges. To evaluate the impact of local temperature rise on E/N reduction we measured thermal dependence of breakdown voltage. By doing so, we were able to evade the contribution of residual plasma species and got direct experimental data on the effect. Finally we made a COMSOL numerical model for residual heat buildup which employed our measured dependence. The model was used to get better insight into the role played by nearby dielectric wall, and allow simple implementation of Navier-Stokes equations into the model.

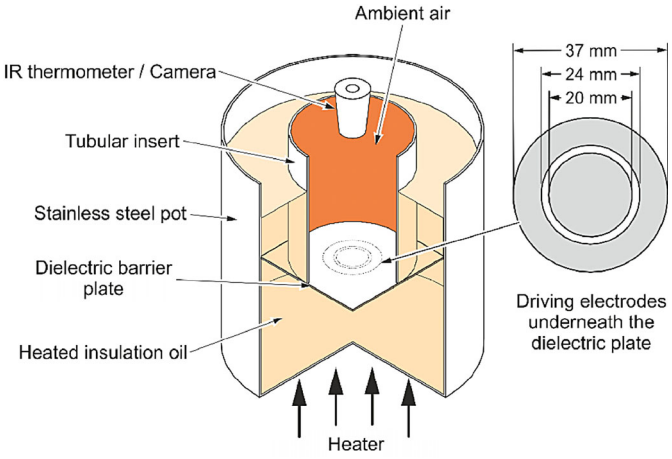

Fig. 1. Schematic cross-cut view of discharge reactor set-up. For the sake of clarity HV feedthroughs and pot lid are omitted from the illustration.

2 Experimental

Coplanar DBD with two concentric circular electrodes was used (Fig. 1). Azimuthal symmetry of discharge electrodes pair eliminated the effect of stray electric field. At the same time, planar geometry of electrodes provided a uniform temperature field across the discharge region; and an unobstructed view for high-speed camera imaging. Measurements were done on 0.635 mm thick AlN (ALUNIT – CeramTec AG) and 96% Al_2O_3 (Elceram a.s.) dielectric plates at driving frequency of 40 kHz in atmospheric pressure air. Relative humidity of air was 30–40% during the meassurements. Therefore the surface of both ceramic materials contained adsorbed water vapor. The diameter of inner circular electrode was 20 mm; inter-electrode gap was 2 mm; outer diameter was 37 mm. Using the hollow metallic cylinder the powered side of coplanar electrode was immersed into insulating oil heat bath (Dow Corning 561 Silicone Transformer Liquid), with the temperature adjustable up to 180 °C by induction cooker Hendi 3500D. Opposite (i.e. discharge) side of electrode was exposed to still ambient air. The temperature of dielectric surface was measured by infrared thermometer OPTCSLT10K (Optris GmbH). Amplitude of feed voltage corresponding to the

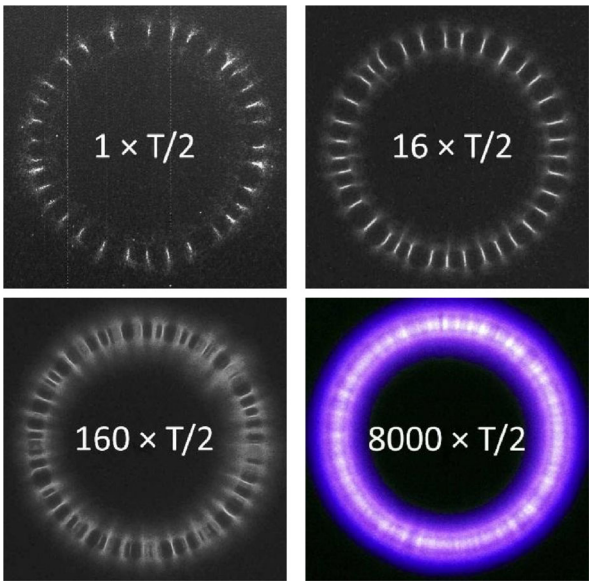

Fig. 2. High-speed camera images for 40 kHz air coplanar discharge on Al_2O_3 with concentric circular electrodes. Individual exposure times were 4 μs, 200 μs, 2 ms and 1/10 s.

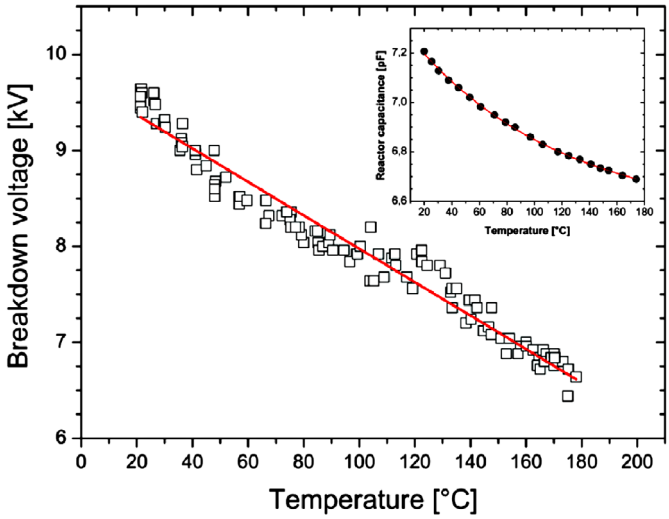

Fig. 3. Temperature dependence of AlN breakdown voltage.

breakdown event was measured by a pair of Tektronix P6015A HV probes attached to Tektronix TDS2024B oscilloscope. In-house built HV generator was modified to allow fine tuning of HV amplitude at fixed frequency. Measurement was done by slow rise of applied voltage at constant rate until the gas breakdown occurred. The moment of breakdown event was detected by triggering oscilloscope with the first discharge current pulse, detected by Pearson 2877 current monitor equipped with capacitive current compensation tool [12] made from and COMET HV vacuum variable capacitor (5−250 pF). After detecting the breakdown event, discharge was turned off and left for 1 min to recover its dielectric surface into initial state. To prevent any hysteresis effect measurements were performed at both temperature rise and temperature fall cycles. Thermal dependence of reactor capacitance was measured by LCR meter HM 8018 (HAMEG Instruments GmbH) at measuring frequency of 25 kHz. The Princeton Instruments PI-MAX 1024RB-25-FG-43 intensified CCD camera (ICCD) equipped with 50 mm, f/2.8 UV lens, and CASIO Exilim F1 digital camera (for high-speed movie recording) were used to detect average residence time of microdischarge channel at the same location.

3 Results

Figure 2 presents visual appearance of discharge at gradually increased exposure times to verify the presence of localized re-appearance in our coplanar arrangement. Owing to its geometrical symmetry discharge took form of multiple (35 ± 2) rather equidistant microfilaments. The maximum number of microfilaments was the same for both tested dielectric materials and was not affected by an increase of applied voltage. Extending camera exposure time over a number of discharge periods allowed documenting a sub-milliseconds discharge patterning. Position of microfilaments remained stable for 40−60 consecutive half-periods (i.e. 0.5−0.8 ms). Afterwards microfilaments had shifted sideways which resulted in the broadening of their trace on the photograph. Recorded high-speed camera movies revealed that the whole ensemble of microfilaments rotated in a fairly regular manner along the circumference of discharge electrode. At longer time-scale (above 200 ms), the patterning became blurred on account of irregularly appearing novel microfilaments within the former inter-filamentary spaces; leading to formation of macroscopically uniform appearance to the naked eye. With respect to the work of reference [2] it is interesting to notice that microfilaments of volume DBD operated at similar conditions (1.2 mm gap; 100 kHz) required as many as 300 consecutive halfperiods to offset their position. An explanation for smaller microfilaments mobility in reference [2] can be: two and half times higher driving frequency comparing to our set-up, which shortened the cooling time between two consequent micro-breakdowns, and the less effective heat dissipation by a dielectric comparing to the coplanar DBD. Both options points out to the importance of heat dissipation.

Figures 3 and 4 show temperature dependence of breakdown voltage for AlN and Al_2O_3 respectively. Both materials exhibited expected breakdown voltage decline with increasing temperature. In case of aluminum nitride AlN the decline was linear with the rate of (17 ± 0.3) V/K. Alumina ceramics (96% Al_2O_3) possessed more complex temperature dependence. Up to 80 °C a strong (almost 30%) reduction of breakdown voltage was present. It was followed by plateau region between 80−130 °C and further breakdown voltage reduction at slower pace compared to the initial one. We have found, by testing several specimen of Al_2O_3 ceramics, that the deviation from linear dependency was a natural material characteristic of our alumina plates. The initial (20−50 °C) and final

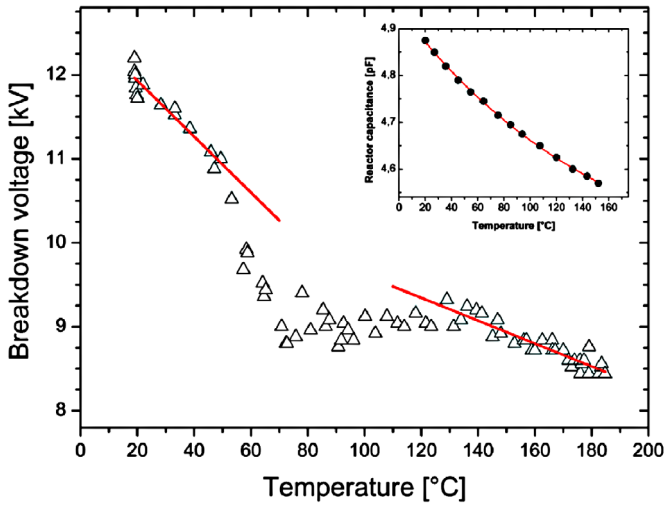

Fig. 4. Temperature dependence of 96% Al_2O_3 breakdown voltage.

(130−180 °C) rates of Al_2O_3 breakdown voltage reduction rate were found to be (34 ± 3) V/K and (13.6 ± 0.1) V/K respectively.

Parasitic effects that might be interfering with our measurements were: electrode geometry changes due to thermal expansion; and changes in dielectric permittivity of involved materials. Manufacturer specified coefficients of thermal expansion are positive and similar for both types of ceramics: $5-7 \times 10^{-6}$ K^{-1}. For temperature change of 150 °C this gives maximum linear expansion of only 0.1% (i.e. 2 μm for our 2 mm gap width). More importantly, the change would have been occurring in the direction which should cause a growth of breakdown voltage, unobserved in our measurements. A possibility of thermal expansion evoking the reduction of breakdown voltage was therefore rejected. Relative permittivity of 96% Al_2O_3 and AlN is known to rise with temperature [13,14]. In coplanar DBD the rise of dielectric permittivity causes local increase of surface electric field strength by refracting its field lines closer to the dielectric surface. This would reduce voltage needed to sustain gas breakdown. Although the rise of dielectric permittivity was expected to be negligible within our temperature range, for the sake of argument we have measured the temperature dependence of reactor capacitance, which is directly proportional to the system dielectric permittivity. As can be seen from insets to Figures 3 and 4, contrary to our expectation the reactor capacitance had been decreasing when temperature grew. We could therefore reject also the possibility of breakdown voltage being reduced by the rise of ceramics plate permittivity. Our further analysis revealed that the decrease of capacitance was due to lowering the permittivity of insulating oil. In contrast to solid dielectrics, the permittivity of insulation oil decreases with rising temperature [15]. However, it follows from the distribution of electric field that the change in oil permittivity does not affect electric field at the opposite side of our discharge dielectric plate.

4 Discussion

Although we found that breakdown voltage reductions are material specific, the reduction coefficient had similar average value of $\kappa \approx 20$ V/K, which was in a good agreement with the following theoretical estimation. At some given value of breakdown reduced electric field $E_b/N = E_b kT/p$, a small rise of temperature ΔT lowers the actual breakdown electric field strength E_b by ΔE_b which obeys:

$$\frac{\Delta E_b}{E_b} = -\frac{\Delta T}{T}.$$

The relation states that for 1 K rise at 300 K we should expect 0.3% smaller electric field strength to initiate a self-sustained discharge. The relative drop in the breakdown electric field strength can be expressed via the relative drop of applied voltage U as follows. The maximum of electric field between two conductive plates can be written as:

$$E = Q\alpha,$$

where Q is total electric charge on conductive plates and α is some geometric factor depending only on suitably chosen spatial coordinates and physical units [16]. This formula comes e.g. from applying Gauss's law to the nearest neighbourhood of conductive plates, where the maximum of E is expected. Employing differentiation chain rule to this formula we can express the change of maximum electric field made by small change of applied voltage U as:

$$\frac{dE}{dU} = \frac{dE}{dQ}\frac{dQ}{dU} = \alpha C,$$

where C states for the system capacitance. By combining both above equations, geometric factor α can be cancelled out and we obtain:

$$\frac{dE}{E} = \frac{\alpha C dU}{Q\alpha} = \frac{dU}{U}.$$

We can see that relative change of electric field strength in the vicinity of electrodes is proportional to the relative change of applied voltage. If we assume that the relative change of local electric field strength is non-sensitive to its actual spatial coordinate, the above expression would hold also for the breakdown field E_b, which is located further away from the electrode of our geometry. Then we can obtain following final formula for the drop of breakdown voltage:

$$\frac{dU_b}{U_b} \approx \frac{\Delta E_b}{E_b} = -\frac{\Delta T}{T}.$$

After substitution we can see that relative reductions on breakdown voltage for 1 K rise at 300 K, i.e. 17 V/9 kV = 0.2% for AlN; 34 V/11.5 kV = 0.3% for Al_2O_3, are in good agreement with predicted ratio of 1 K/300 K = 0.3%.

Gas expansion time evaluated as the ratio of the channel radius to the sound velocity was $\tau = 600$ ns, therefore we might safely exclude shock waves from our

considerations, and assume, that at 40 kHz driving frequency the microdischarge of the subsequent half-period would be affected only by a local reduction of gas density due to the temperature rise. Application of calorimetry formula to the volume of our microfilament ($L = 2$ mm; $2R = 0.2$ mm) being ohmically heated by 9×10^{-6} J of single current pulse, resulted in an estimated increase of microfilament average temperature by $\Delta T \sim 100$ K. Such value was consistent e.g. with earlier estimation of reference [17], where $\Delta T < 40-100$ K had been stated. However, for the train of re-occurring microfilaments this temperature increment should gradually slow down. Firstly there will be an enhanced heat flux due to the growth of temperature gradient. Secondly the drop of breakdown voltage U_b would inevitably cause also some drop in dissipated electric power, which is proportional to the square of U_b.

Using the COMSOL simulation software we made a numerical calculation of such train of reoccurring microfilaments, to take an account for the rate at which microfilaments' channel temperature converges to its final temperature, and to assess its actual magnitude. A microfilament was modelled as an air column ($L = 2$ mm, $2R = 0.2$ mm) located in a free space, at initial temperature of 300 K, periodically heated by 10 ns pulses at 2×40 kHz repetition rate. The heat source was modelled to have a Gaussian profile with $\sigma = 0.05$ mm, which corresponded to 95% of heating power being dissipated within the microfilament's 0.2 mm diameter. Energy per pulse was calculated from known breakdown voltage at average temperature of microfilament's channel and from the electrode capacitance per single microfilament. For higher temperatures the breakdown voltage was extrapolated from our measured linear dependency of U vs. T for AlN (i.e. $\kappa = 17$ V/K). Simulation was made for AlN only since it possessed more simple thermal dependence of breakdown voltage.

Figure 5 shows the saw-like pattern of average temperature growth. Initial burst of temperature by the instant 10 ns release of heating is followed by gradual decline due to the thermal dissipation. One can clearly see that in approximately 20 repetition cycles the microfilament reached a quasi-stable temperature of approximately 500−550 K. This value is in good agreement with the peak rotational temperature of 600 ± 20 K, determined from second positive system of nitrogen for microfilament at equivalent geometry of coplanar DBD [18]. At atmospheric pressure T_{rot} is considered to be an appropriate estimation of neutral gas temperature [19]. The simulation allowed us to evaluate the effect of convective heat transfer by its comparison with purely conductive heat transfer model. Gas convection allowed faster transfer of heated gas from the centre of microfilament to its borders, which contributed to the higher average temperature of microfilament channel. Obtained difference in the range of 10 K was not significant however.

The rise of temperature to 550 K represents local reduction of breakdown voltage almost to the half of its initial room temperature value. In such a way the residual heat built-up alone is capable of spatially stabilizing the

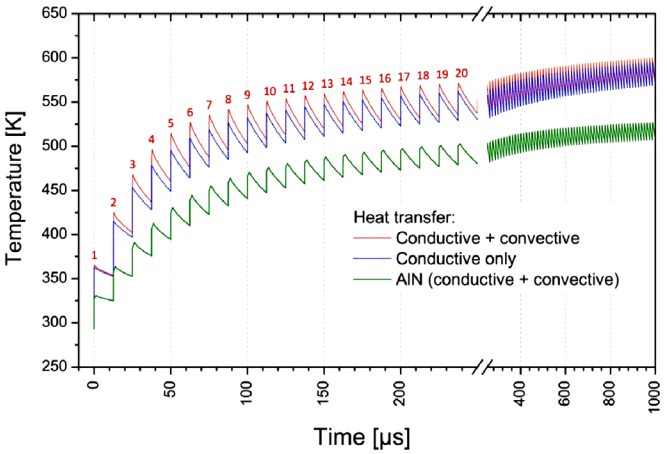

Fig. 5. Simulation of average temperature inside microfilament's column volume, built by the train of re-occurring localized breakdowns.

microfilament. However, whether the sole "heat" scenario could be carried out is determined by actual performance of the first few of microdischarges. As it can be seen from the modelled data in Figure 5, first microfilament delivered more than 50 K of average local temperature increase to its subsequent follower. This corresponds to almost 10% reduction of local breakdown voltage. Referring to our analysis in the Introduction section, even a lesser relative reduction represents a substantial comparative advantage over the adjacent microdischarges, when their extremely short lifetime is taken into account. Unfortunately there is a lack of experimental data, chiefly due to the detection limits of currently available spectroscopic techniques, which could directly confirm our predicted step-wise temperature additions at this magnitude and time scale. With this respect, the most straightforward experiments would in our opinion involve some adaptation of laser schlieren deflectometry [20].

Paradoxically, spatial stabilization leading through the thermal build-up to the formation of quasi-stable temperature of microfilament is responsible also for its observed lateral drift. Figure 6 shows temporal development of radial temperature profile of re-occurring localized microfilaments. Quasi-stable temperature is first reached at the centre of microfilament, from where it spreads radially according to the heat transfer constants of working gas. When the quasi-stable temperature is reached (i.e. in approximately 20 repetition cycles), the half-width of volume occupied by heated gas is almost twice of the initial microfilament. Therefore, owing to the stochastic nature of discharge formation, the probability of discharge appearance at slightly offset position to its predecessor is increased as well; and continues to rise with further radial spreading of residual heat build-up. At this point it is appropriate to notice, that the used thermal diffusivity coefficient is similar in magnitude to the mass diffusivity of molecules involved (10^{-5} m^2/s). Therefore the modelled radial expansion of thermal profile corresponds also to the radial expansion of plasma formed active species;

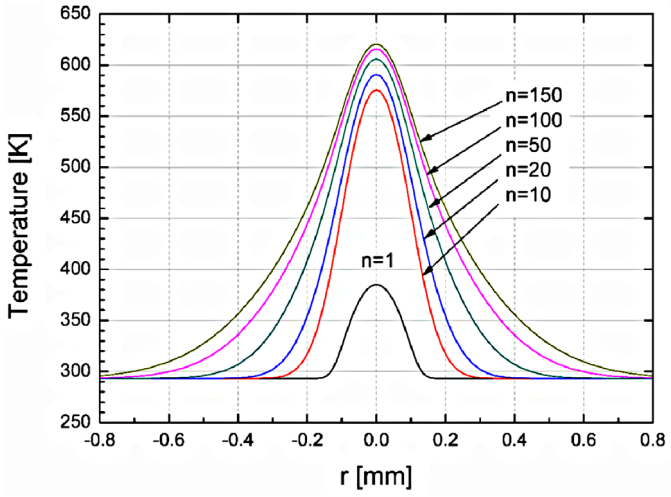

Fig. 6. Simulated radial temperature profile resulting from the train of re-occurring microfilaments, immediately before the $(n+1)$th breakdown.

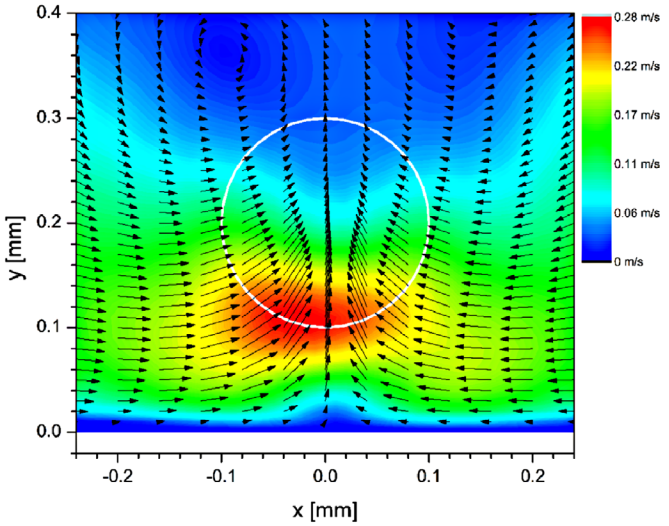

Fig. 7. Simulated velocity field of microfilament at the vicinity of dielectric wall (AlN) after the train of 150 localized breakdowns. Position of microfilament is indicated by white circle. Wall is situated at $y = 0$.

providing that there is some quasi-stable concentration reached over several tens of initial repetition cycles. In that case the probability of lateral drift would be further enhanced by the growth of volume with a uniformly enhanced production of seed electrons.

As a final point we have attempted to evaluate the role of dielectric plate (with its 10^3 higher thermal conductivity comparing to any gas) in the model of coplanar DBD geometry. Free space environment of our volume DBD model was replaced by infinite wall of AlN, placed at normal distance of 0.2 mm from the microfilament's central axis. As can be seen in Figure 7, the presence of dielectric wall introduced a thermal body force acting on the microfilament's channel in the normal direction away from the wall; causing a gas flow at velocities of 0.3 m/s. The body force originated from the temperature asymmetry in the normal direction as shown in Figure 8a. Highly conductive wall provided an effective cooling of its adjacent region. Thus the region of higher temperature (hence lower gas density) can move only away from the wall, creating the pressure difference in this direction. Figure 8a also shows that the position of peak temperature drifted in normal direction as well, which in real situation would mean its drift to the space of lower electric field. Our COMSOL numerical model however did not take into account this effect. In the direction parallel to the wall (lateral direction) the temperature profile remained symmetric (Fig. 8b), although its lateral spreading slightly lagged behind the spreading of free microfilament of Figure 6. As can be seen from Figure 5, heat dissipation of wall reduced also the absolute value of quasi-stable temperature to which the microfilaments train approaches by some 100 K. Nevertheless, the pace at which this quasi-equilibrium was established remained unaffected.

It can be concluded that the model pointed out the necessity of introducing a hydrodynamic aspect into consideration when analyzing the stability of coplanar DBD or surface DBD in general. Although the general dynamics of process leading to eventual quasi-stable temperature is similar, coplanar microfilament is inherently less stable due to the asymmetric nature of acting thermal body force.

5 Conclusion

Our experiments confirmed a theoretically predicted temperature reduction of DBD breakdown voltage, being in the order of 20 V/K. Due to the insufficient rate of heat dissipation between two consecutive half-periods, lower gas density in the residual heat trace is sufficient to promote local breakdown at lower applied voltage. The effect appears to be significant even for the first breakdown pulse; therefore microfilament can be spatially stabilized by the residual heat buildup alone. At the same time, there is a quasi-stable temperature to which the microfilament channel temperature rapidly converges. Its modelled amplitude agrees well with formerly determined rotational temperature of coplanar DBD microfilaments. The existence of quasi-stable temperature offers a natural explanation for the observed lateral drift of DBD microfilaments. As the channel of favoured breakdown condition is growing in diameter the breakdown probability is equalized within its interior. Our results imply that quasi-stable temperature should be taken as a more adequate background gas temperature when modelling chemical processes within the microfilament's channel. The proximity of dielectric wall to microfilament's channel affects the symmetry of its temperature profile, giving rise to the thermal body force. It provides a natural explanation for known lower spatial stability of coplanar DBD microfilaments in comparison to microfilaments of volume DBD.

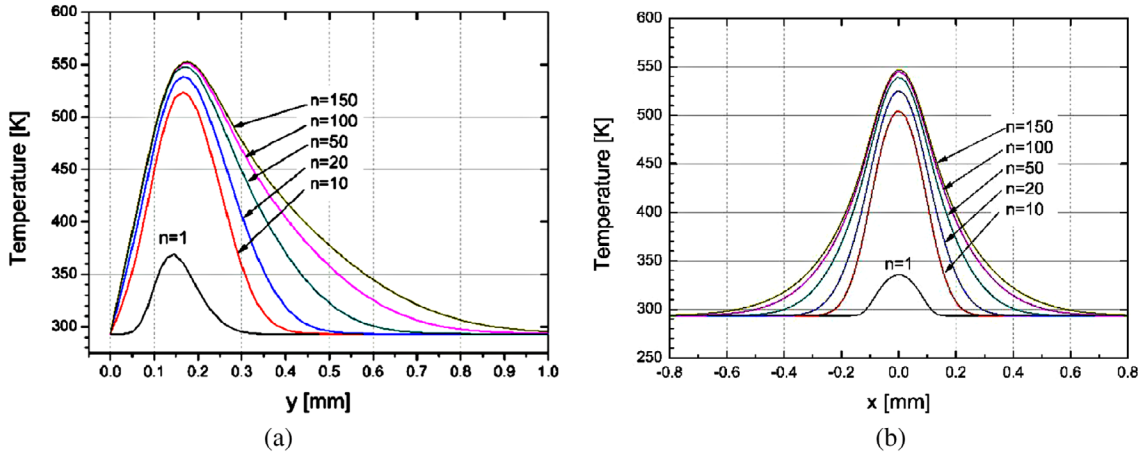

Fig. 8. Simulated temperature profiles resulted from the train of re-occurring microfilaments above AlN surface in: (a) normal; (b) parallel direction to the wall; immediately before the $(n+1)$th breakdown.

Author contribution statement

J.R. initiated the project, supervised it and wrote the manuscript. Z.S. carried out the measurement of breakdown voltage temperature dependence. T.M. made high speed camera characterization of microfilament spatial stability. J.Č. performed COMSOL modeling. J.R. and J.Č. jointly interpreted the results. All authors commented on the manuscript.

This work was supported by the Czech Science Foundation, Project No. GA13-24635S. This research has been supported by the Project CZ.1.05/2.1.00/03.0086 funded by European Regional Development Fund and Project LO1411 (NPU I) funded by Ministry of Education Youth and Sports of Czech Republic.

References

1. Yu. Akishev, G. Aponin, A. Balakirev, M. Grushin, V. Karalnik, A. Petryakov, N. Trushkin, Acta Technica **56**, T3 (2011)
2. Yu. Akishev, G. Aponin, A. Balakirev, M. Grushin, V. Karalnik, A. Petryakov, N. Trushkin, Eur. Phys. J. D **61**, 421 (2011)
3. Yu. Akishev, G. Aponin, A. Balakirev, M. Grushin, V. Karalnik, A. Petryakov, N. Trushkin, Plasma Sources Sci. Technol. **20**, 024005 (2011)
4. Yu.V. Yurgelenas, H.-E. Wagner, J. Phys. D **39**, 4031 (2006)
5. T. Callegari, B. Bernecker, J.P. Boeuf, Plasma Sources Sci. Technol. **23**, 054003 (2014)
6. J. Čech, J. Hanusová, P. Sťahel, M. Černák, Open Chem. **13**, 528 (2015)
7. Y.P. Raizer, *Gas discharge physics* (Springer-Verlag, Berlin, 1997), p. 222, Eq. (9.8)
8. G.V. Naidis, J. Phys. D **41**, 234017 (2008)
9. F. Tholin, A. Bourdon, J. Phys. D **46**, 365205 (2013)
10. J.A. Riousset, V.P. Pasko, A. Bourdon, J. Geophys. Res. Space, **115**, A12321 (2010)
11. V.I. Gibalov, G.J. Pietsch, Plasma Sources Sci. Technol. **21**, 024010 (2012)
12. J.R. Roth, J. Rahel, X. Dai, D.M. Sherman, J. Phys. D **38**, 555 (2005)
13. L.Y. Chen, in *ICEPT 2007 – 8th International Conference on Electronic Packaging Technology*, 14–17 Aug. 2007, p. 1
14. J.S. Thorp, D. Evans, M. Al-Naief, M. Akhtaruzzaman, J. Mater. Sci. **25**, 4965 (1990)
15. R. Bartnikas, IEEE Trans. Elect. Insul. **EI-2**, 33 (1967)
16. M. Anandan, R.P. Wadhwa, S. Mandavilli, K.R. Savoor, IEEE Trans. Electron Devices **28**, 1035 (1981)
17. D. Braun, U. Kuchler, G. Pietsch, J. Phys. D **24**, 564 (1991)
18. J. Čech, P. Sťahel, Z. Navrátil, Eur. Phys. J. D **54**, 259 (2009)
19. P.J. Bruggeman, N. Sadeghi, D.C. Schram, V. Linss, Plasma Sources Sci. Technol. **23**, 023001 (2014)
20. J. Schäfer, Z. Bonaventura, R. Foest, Eur. Phys. J. Appl. Phys. **71**, 20804 (2015)